Computational Methods of Solid Mechanics

Project report

Due on Dec. 16, 2015

Prof. Allan F. Bower

Weilin Deng

Simulation of adhesive contact with molecular potential

1 Project description

In the project, we will investigate the adhesive contact between a soft tip with rough surface and a rigid substrate, see Fig. 1(a). Since the tip size is much smaller than the substrate, we take the substrate to be semi-infinite. The profile of the rough surface of tip in the reference configuration is given by

$$x_2(x_1) = \frac{x_1^2}{2R} + A\left[1 - \cos\left(\frac{2\pi x_1}{\lambda}\right)\right] \tag{1}$$

where the first term is a parabola shape with maximum curvature R and the second term is a sinusoid undulation with wavelength λ and amplitude A. We take $\lambda, A \ll R$ to represent the small scale roughness of the surface. The tip material is described by Neo-Hookean model as discussed in the class. We model the adhesive contact behavior by assuming that the tip and substrates material points interact with one another through the Lennard-Jones type interaction potential

$$V_{LJ} = 4\epsilon\left[-\left(\frac{\sigma}{r}\right)^6 + \left(\frac{\sigma}{r}\right)^{12}\right] \tag{2}$$

where ϵ and σ are constants and have units of energy and length respectively, r is the distance between two points. The interaction force between the tip and substrate material point is obtained by differentiating the interaction potential. Since the substrate is semi-infinite large and rigid, the body force acted on the tip material point and the work of adhesion of the material can be derived analytically. Due to symmetry, the only nonzero component of body force is

$$b_2(\underline{\mathbf{y}}) = 4\pi\epsilon\sigma^2\rho_s\rho_t(\underline{\mathbf{y}})\left[\frac{1}{5}\left(\frac{\sigma}{y_2}\right)^{10} - \frac{1}{2}\left(\frac{\sigma}{y_2}\right)^4\right] \tag{3}$$

as shown in Fig. 1(b), where ρ_t and ρ_s are the tip and substrate densities. The work of adhesion is

$$w = \frac{1}{4}\left(\frac{2}{15}\right)^{1/3}\pi\epsilon\rho_s\rho_t\sigma^4 \tag{4}$$

Note that the body force is described in the deformed configuration. Rewrite eq. 3 in the reference configuration we have

$$b_2(\underline{\mathbf{x}}) = 4\pi\epsilon\sigma^2\rho_s\rho_t^0 J^{-1}(\underline{\mathbf{x}})\left[\frac{1}{5}\left(\frac{\sigma}{x_2+u_2}\right)^{10} - \frac{1}{2}\left(\frac{\sigma}{x_2+u_2}\right)^4\right] \tag{5}$$

where u_2 is the displacement in $\hat{e}_2$ direction.

2 Governing equations

The equilibrium equation in the deformed configuration is

$$\begin{aligned} \frac{\partial\sigma_{ij}}{\partial y_j} + b_i = 0 \quad &\text{in} \quad V \\ \sigma_{ij}n_j = t_i^* \quad &\text{on} \quad S_2 \\ u_i = u_i^* \quad &\text{on} \quad S_1 \end{aligned} \tag{6}$$

where σ_{ij} is the Cauchy stress. Let η_i be the test function with $\eta_i = u_i^*$ on S_1. The weak form is

$$\int_V \sigma_{ij}\frac{\partial\eta_i}{\partial y_j}\,dV - \int_V b_i\eta_i\,dV - \int_{S_2} t_i^*\eta_i\,dA = 0 \tag{7}$$

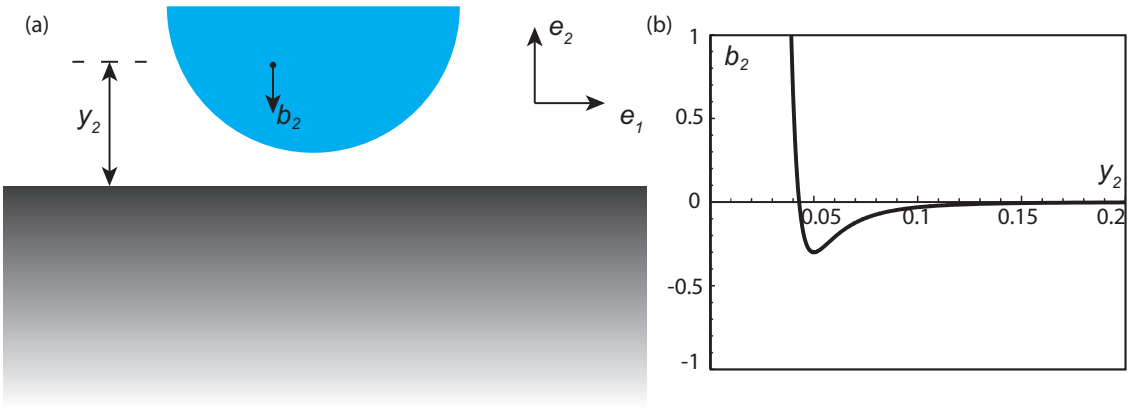

Figure 1: (a) The schematic of adhesive contact between the soft indenter and semi-infinite rigid substrate and (b) the Lennard-Jones type body force.

Map the integral over the deformed configuration to the reference configuration we have

$$\int_{V_0} \tau_{ij} \frac{\partial \eta_i}{\partial y_j} \, dV_0 - \int_{V_0} b_i^0 \eta_i \, dV_0 - \int_{S_2^0} t_i^0 \eta_i \, dA_0 = 0 \tag{8}$$

where $\tau_{ij} = J \cdot \sigma_{ij}$ is the Kirchoff stress, $b_i^0 = J \cdot b_i$, and t_i^0 is the traction mapped back to the reference configuration. In the project, the body force is dependent on the position as described by eq. 5, and for simplicity, the traction boundary condition is not considered. Hence the third term on the left hand side of the weak form is zero.

3 FE implementation

Introduce FE intepolation

$$u_i = N^a(\underline{\mathbf{x}}) u_i^a, \quad \eta_i = N^a(\underline{\mathbf{x}}) \eta_i^a \tag{9}$$

Substitute into the weak form we obtain

$$R_i^a[u_k^b] + B_i^a[u_k^b] = F_i^a \tag{10}$$

where

$$\begin{aligned} R_i^a &= \int_{V_0} \tau_{ij}[B_{kl}] \frac{\partial N^a}{\partial y_j} \, dV_0 \\ B_i^a &= -\int_{V_0} b_i^0 N^a \, dV_0 \\ F_i^a &= \int_{S_2^0} t_i^0 N^a \, dA_0 \end{aligned} \tag{11}$$

Note that the force vector B_i^a is now a function of displacement since the body force is nonuniform distributed given by

$$b_i^0 = 4\pi\epsilon\sigma^2 \rho_s \rho_t^0 \delta_{i2} \left[\frac{1}{5} \left(\frac{\sigma}{x_i + u_i} \right)^{10} - \frac{1}{2} \left(\frac{\sigma}{x_i + u_i} \right)^4 \right] \tag{12}$$

No summation of i here. The nonlinear equation will be solved using Newton-Raphson iteration. Start with initial guess w_i^a and try to correct the guess with correction dw_i^a. Linearizing eq. 10 in dw_i^a yields a system of linear equation

$$(K_{aibk}^R + K_{aibk}^F) dw_k^b = -R_i^a - B_i^a + F_i^a \tag{13}$$

to solve for dw_i^a, where the term K^R_{aibk} is the usual one we derived in the class. The new term K^B_{aibk} appearing in the stiffness matrix is

$$K^B_{aibk} = \frac{\partial B_i^a}{\partial u_k^b} = -\int_{V_0} \frac{\partial b_i^0}{\partial u_k^b} N^a \, dV_0 \tag{14}$$

Everything is familar except the new term we need to take care of. The FE procedure will be implemented with UEL in ABAQUS.

Let us denote

$$f(y_i) = \frac{1}{5}\left(\frac{\sigma}{y_i}\right)^{10} - \frac{1}{2}\left(\frac{\sigma}{y_i}\right)^{4} \tag{15}$$

To avoid $f(y_i)$ goes to infinity as $y_i = 0$, we can set the body force to the following form:

$$b_i^0 = \begin{cases} \delta_{i2} c_0 f(y_i), & y_i \geq \Delta \\ \delta_{i2} c_0 \left[h + k \cdot (y_i - \Delta)\right], & y_i < \Delta \end{cases} \tag{16}$$

where $c_0 = 4\pi\epsilon\sigma^2\rho_s\rho_t^0$, Δ is a very small positive parameter. For example, we can take $\Delta = 0.5\sigma$, and

$$\begin{aligned} h &= f|_{y_i=\Delta} = \frac{984}{5} \\ k &= \frac{df}{dy_i}|_{y_i=\Delta} = -\frac{4032}{\sigma} \end{aligned} \tag{17}$$

Therefore, for $y_i \geq \Delta$,

$$B_i^a = -\int_{V_0} \delta_{i2} c_0 \left[\frac{1}{5}\left(\frac{\sigma}{x_i + u_i}\right)^{10} - \frac{1}{2}\left(\frac{\sigma}{x_i + u_i}\right)^{4}\right] N^a \, dV_0 \tag{18}$$

and

$$K^B_{aibk} = -\int_{V_0} \delta_{2k} c_0 \left[\frac{2\sigma^4}{(x_i + u_i)^5} - \frac{2\sigma^{10}}{(x_i + u_i)^{11}}\right] N^a N^b \, dV_0 \tag{19}$$

For $y_i < \Delta$,

$$B_i^a = -\int_{V_0} \delta_{i2} c_0 \left[h + k \cdot (y_i - \Delta)\right] N^a \, dV_0 \tag{20}$$

and

$$K^B_{aibk} = -\int_{V_0} \delta_{2k} c_0 k \cdot N^a N^b \, dV_0 \tag{21}$$

4 Benchmarks

In this section, we verify the UEL subroutine by several simple test cases. In cases 1-3, the simple body forces (Fig. 2(b-d)) are applied to a single element (1×1 in size), which is specified with a rigid body motion in the -$\hat{e}_2$ direction (Fig. 2(a)). The body forces have the form

$$\begin{aligned} &\text{Case 1:} \quad b_2 = 1.0 \\ &\text{Case 2:} \quad b_2 = \begin{cases} 0, & r > r_0 \\ 1.0 - \frac{r}{r_0}, & 0 < r < r_0 \\ 1.0, & r < 0 \end{cases} \\ &\text{Case 3:} \quad b_2 = \begin{cases} 0, & r > 3r_0 \\ -3.0 + \frac{r}{r_0}, & 2r_0 < r < 3r_0 \\ 1.0 - \frac{r}{r_0}, & 0 < r < 2r_0 \\ 1.0, & r < 0 \end{cases} \end{aligned} \tag{22}$$

The parameter r_0 is set to be 1.0. The total reaction force of the element, for the three cases, is shown in Fig. 3, which is the same as the exact solution. The total force is negative since a positive body force is applied.

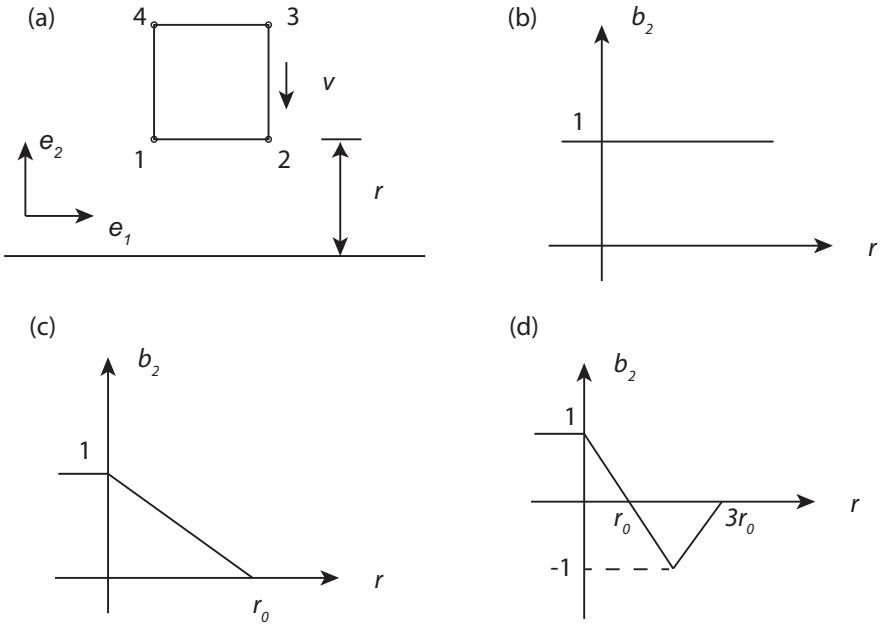

Figure 2: Schematic of element test with three simple body forces.

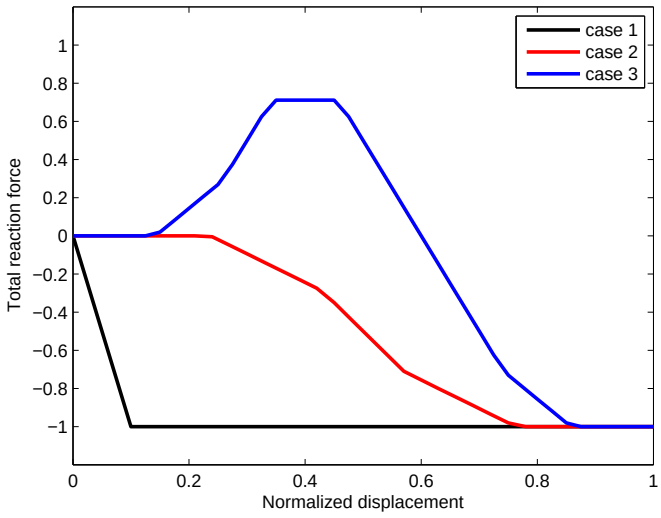

Figure 3: The reaction force F_2 of the element with rigid body motion in test cases 1-3.

In test case 4, we compare the Hertz contact simulation of the body force method with that in ABAQUS/CAE. The contact of a elastic indenter of radius 2.5 with rigid substrate is simulated. A indent depth of 0.02 is applied. The Young's modulus E and Poisson's ratio μ are set to be 2000.0 and 0.3. Theoretically, the contacting surface cannot penetrating each other. Hypothetically, it can be viewed as a infinite force is

applied on these surface. Therefore, the body force has the form

$$b_2 = \begin{cases} 0, & r > 0 \\ k \cdot r, & r < 0 \end{cases} \tag{23}$$

where $-k$ is a large number.

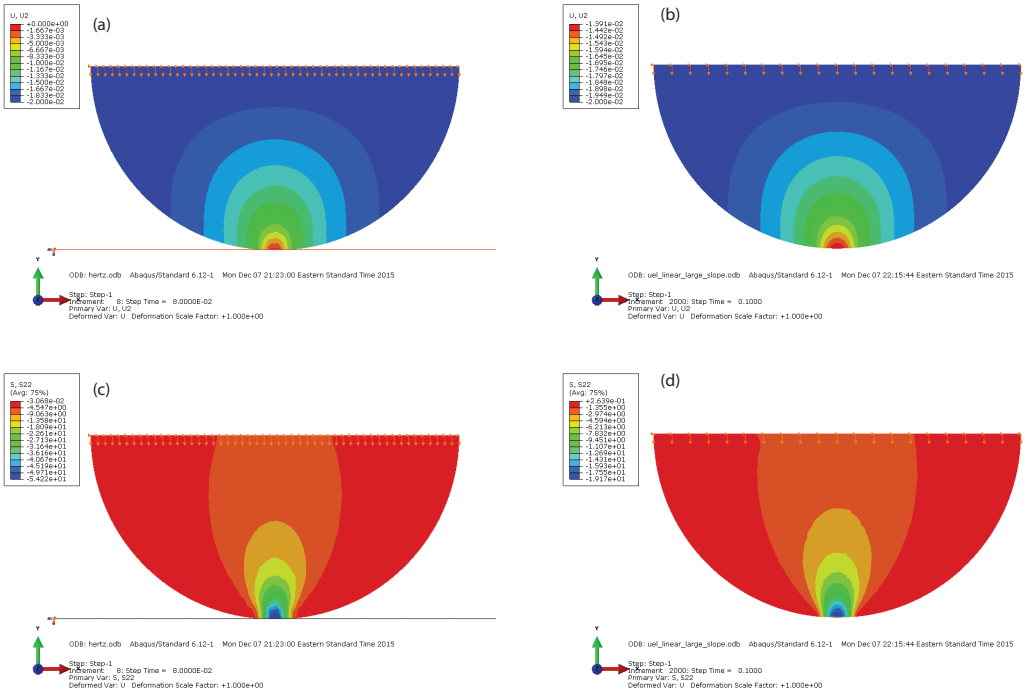

Figure 4: The comparison of u_2 and σ_{22} of ABAQUS/CAE (a,c) and body force method for $k = -200$ (b,d) in the Hertz contact simulation.

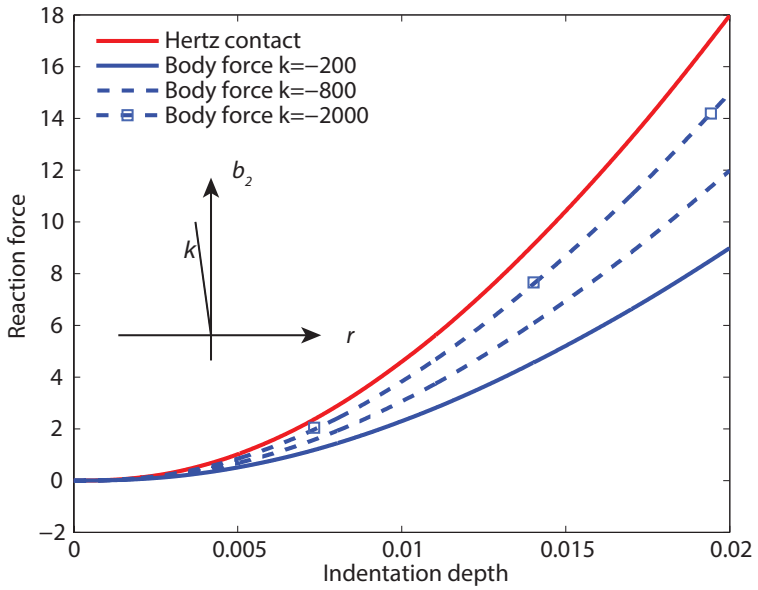

Figure 5: The comparison of force-depth curves of Hertz contact of ABAQUS/CAE and body force method.

Fig. 4 shows the comparison of u_2 and σ_{22} plots calculated from ABAQUS/CAE and the body force method with $k = -200$. As we can see, the distribution of u_2 and σ_{22} is the same, but the magnitude is different. The result of body force method converges to that of ABAQUS/CAE as the slope k decreases. This is reflected in the comparison of force-depth curves, as shown in Fig. 5. As the slope k decreases from -200 to -2000, the difference of force-depth curve of ABAQUS/CAE and body force method becomes smaller and smaller.

5 Adhesive contact

In this section, we study the adhesive contact through the method of Lennard-Jones type body force, as descried in Sec. 1. As predicted by JKR theory, there exist "pull-in" and "pull-off" instabilities during the loading and unloading of the tip due to the adhesive interactions. To overcome the convergence problem in the numerical simulation, a "viscosity" term is added to the body force, i.e.,

$$b_i^0 = \delta_{i2} c_0 \left[\frac{1}{5} \left(\frac{\sigma}{x_i + u_i} \right)^{10} - \frac{1}{2} \left(\frac{\sigma}{x_i + u_i} \right)^{4} \right] \left(1 + \eta \frac{du_i}{dt} \right). \tag{24}$$

where η is a small number. Accordingly, the force vector B_i^a and stiffness matrix K_{aibk}^B become

$$B_i^a = - \int_{V_0} \delta_{i2} c_0 \left[\frac{1}{5} \left(\frac{\sigma}{x_i + u_i} \right)^{10} - \frac{1}{2} \left(\frac{\sigma}{x_i + u_i} \right)^{4} \right] \left(1 + \eta \frac{\Delta u_i}{\Delta t} \right) N^a \, dV_0 \tag{25}$$

and

$$\begin{aligned} K_{aibk}^B = & - \int_{V_0} \delta_{2k} c_0 \left[\frac{2\sigma^4}{(x_i + u_i)^5} - \frac{2\sigma^{10}}{(x_i + u_i)^{11}} \right] \left(1 + \eta \frac{\Delta u_i}{\Delta t} \right) N^a N^b \, dV_0 \\ & - \int_{V_0} \delta_{2k} c_0 \left[\frac{1}{5} \left(\frac{\sigma}{x_i + u_i} \right)^{10} - \frac{1}{2} \left(\frac{\sigma}{x_i + u_i} \right)^{4} \right] \frac{\eta}{\Delta t} N^a N^b \, dV_0 \end{aligned} \tag{26}$$

In the simulation, a 2D tip is moving in the -$\hat{e}_2$ direction and subjected to the body force as described by Eq. 24. The parameters σ and η are taken to be 10 nm and 0.01, respectively. The parameters Δ and k are taken to be 0.5σ and 0. The material is described by Neo-Hookean model. The shear modulus is 0.5 MPa. The work of adhesion of the material is ~ 1 mJ/m^2. Equivalently, the constant c_0 is taken to be 3.132×10^2. The force-displacement curve during the loading is shown in Fig. 6. As we can see, as the the force decreases suddenly at a critical point when the "pull-in" instability occurs. Then the force increases as the indent depth increases. The contour plot of σ_{22} after the "pull-in" instability is shown in Fig. 7.

Remark: The convergence is a big issue in this project. The mesh should be very refined to be able to resolve the body force field. Although the "pull-in" instability is captured in the loading process, the computation does not converge during the unloading process, hence the "pull-off" instability is not shown in the result. A more plausible way is to do the dynamic simulation by using VUEL subroutine.

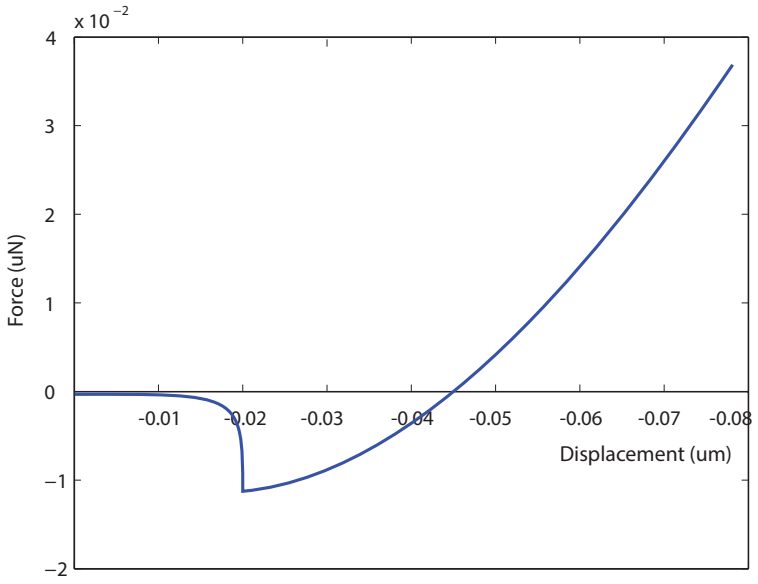

Figure 6: The force-displacement curve of the adhesive contact.

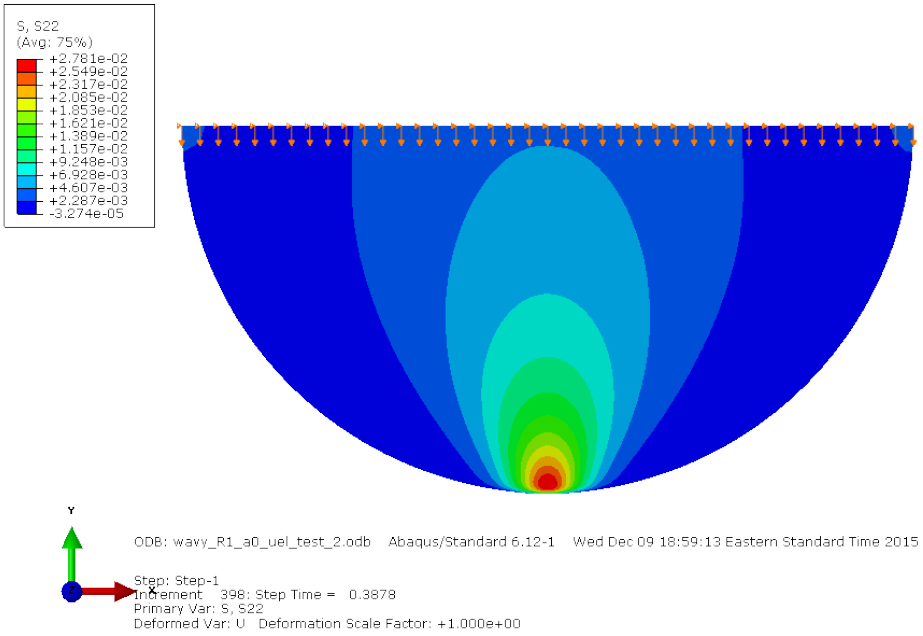

Figure 7: The contour plot of σ_{22} after the "pull-in" instability.